Vibronic eigenstates and the geometric phase effect in the 2 E″ state of NO 3

Wolfgang Eisfeld, Alexandra Viel

Vibronic eigenstates and the geometric phase effect in the $^2E''$ state of NO_3

Wolfgang Eisfeld and Alexandra Viel

Citation: J. Chem. Phys. **146**, 034303 (2017); doi: 10.1063/1.4973983
View online: http://dx.doi.org/10.1063/1.4973983
View Table of Contents: http://aip.scitation.org/toc/jcp/146/3
Published by the American Institute of Physics

Vibronic eigenstates and the geometric phase effect in the $^2E''$ state of NO_3

Wolfgang Eisfeld[1,a)] and Alexandra Viel[2,b)]
[1]*Theoretische Chemie, Universität Bielefeld, Postfach 100131, D-33501 Bielefeld, Germany*
[2]*Institut de Physique de Rennes, CNRS and Université de Rennes 1, UMR 6251, F-35042 Rennes, France*

(Received 14 June 2016; accepted 31 December 2016; published online 19 January 2017)

The $^2E''$ state of NO_3, a prototype for the Jahn-Teller effect, has been an enigma and a challenge for a long time for both experiment and theory. We present a detailed theoretical study of the vibronic quantum dynamics in this electronic state, uncovering the effects of tunnelling, geometric phase, and symmetry. To this end, 45 vibronic levels of NO_3 in the $^2E''$ state are determined accurately and analyzed thoroughly. The computation is based on a high quality diabatic potential representation of the two-sheeted surface of the $^2E''$ state developed by us [W. Eisfeld *et al.*, J. Chem. Phys. **140**, 224109 (2014)] and on the multi-configuration time dependent Hartree approach. The vibrational eigenstates of the NO_3^- anion are determined and analyzed as well to gain a deeper understanding of the symmetry properties of such D_{3h} symmetric systems. To this end, 61 eigenstates of the NO_3^- anion ground state are computed using the single sheeted potential surface of the $^1A_1$ state published in the same reference quoted above. The assignments of both the vibrational and vibronic levels are discussed. A simple model is proposed to rationalize the computed NO_3 spectrum strongly influenced by the Jahn-Teller couplings, the associated geometric phase effect, and the tunnelling. Comparison with the available spectroscopic data is also presented. *Published by AIP Publishing.* [http://dx.doi.org/10.1063/1.4973983]

I. INTRODUCTION

Nonadiabatic couplings among electronic states play a crucial role in many photochemical processes and often in the spectroscopy of electronically excited states. Thus, the nonadiabatic dynamics of such chemical systems is a fascinating topic and its fundamental understanding is of considerable significance. A particularly interesting situation is the presence of conical intersections and the resulting breakdown of the Born-Oppenheimer (BO) approximation, which is of great interest.[1] This means that the nuclear and electronic degrees of freedom are coupled inseparably, which has to be accounted for in any reasonable theoretical treatment.

A time-tested procedure to treat a molecular system theoretically is to first solve the electronic problem for fixed nuclear geometries and then generate a single potential energy surface (PES), which is finally used to solve the nuclear problem on this potential. However, the breakdown of the BO approximation requires changing this scheme and computing several electronic states for fixed geometries, then generating a PES model that includes the state-state couplings induced by the nuclear motions, and finally solving the nuclear problem simultaneously on a coupled set of PESs. It is established by now that a diabatic or rather *quasi*-diabatic representation of the electronic Hamiltonian and corresponding PES matrix is of considerable advantage in this scheme.[1–12] Unfortunately, most diabatic models like the ones based on the tremendously successful linear vibronic coupling method[13] are limited to processes that are dominated by short-time dynamics. In this case, only a rather small part of the coupled PESs is of significance and needs to be described qualitatively correctly. Many processes like nonadiabatic reactions or the dynamics underlying strongly perturbed yet well resolved spectra are not of this kind and do require accurate coupled PESs over an extended region of nuclear configuration space. For this reason, we and others have been developing methods to diabatize electronic structure data[14–28] and to generate and represent coupled PESs that are accurate over a larger range of nuclear configurations.[29–54] We recently applied our methodology to the development of a highly accurate diabatic representation of the first excited electronic state $^2E''$ of NO_3, which is a prototypical Jahn-Teller system in which the proper treatment of the direct dissociation asymptotes is very important.[55] In the present study, we utilize this PES model for a detailed analysis of the nuclear dynamics in the $^2E''$ state.

Our system of choice, the nitrate radical (NO_3), offers a wide range of complications and makes it an ideal and rigorous test case of our methodology.[42,55] There is also considerable interest in this radical due to its importance in atmospheric chemistry,[56] which we will not focus on in the context of the present study. The first problem is the very complicated electronic structure that requires special treatments to avoid artifacts. Even the electronic ground state is not easily computed by standard *ab initio* methods due to a very strong tendency for the artificial symmetry-breaking of the electronic wave function.[57] The first two excited states are both doubly degenerate, giving rise to fairly strong Jahn-Teller couplings and the second excited state interacts strongly with the ground state by the *pseudo*-Jahn-Teller coupling. A reliable computation of the adiabatic PESs of this system requires a fairly elaborate and computationally demanding

a)wolfgang.eisfeld@uni-bielefeld.de
b)alexandra.viel@univ-rennes1.fr

multireference configuration interaction (MRCI) treatment of the first five electronic states.[58] A single-reference treatment of the dissociative PESs is inappropriate and will lead to artifacts and qualitatively wrong results.[59] The vibronic coupling problem of the ground state has been treated successfully before[60–62] but no extended PES has been developed. The treatment of the first excited state was by far less satisfactory[63–66] until very recently.[55] This first excited state of $^2E''$ symmetry, though predicted before theoretically,[67] was first observed in a photoelectron detachment spectrum in 1991.[68] Much later it was also measured in direct absorption by gas phase cavity ring-down spectroscopy (CRDS)[69–72] as well as in a neon matrix at 4.3 K.[73] These spectra are fairly resolved but show very complicated line patterns due to the strong nonadiabatic interactions. Thus, such spectra are an excellent test for the accuracy of the coupled surfaces developed in our previous work[55] and also will provide a lot of insights into the nonadiabatic dynamics underlying such spectra.

In order to understand the absorption spectra, we study in detail the vibronic levels corresponding to the isolated $^2E''$ electronic state of NO_3. The Jahn-Teller effect active in this state and the corresponding conical intersection result in the phenomenon of the geometric phase effect within the adiabatic representation.[74] This effect together with the special shape of the lower adiabatic PES, showing three equivalent potential wells, which induces tunneling, have a strong impact on the level structure of the vibronic eigenstates in the $^2E''$ manifold. We rationalize the corresponding effects by a simple model and compare the derived predictions with the computed vibronic eigenstates using our diabatic PES model. For comparison, we also compute the eigenstates for the NO_3^- ground state, which does not present any Jahn-Teller or geometric phase effect. We finally use the insights from the theoretical NO_3 model assisted by insights from the anion calculations to assign the computed eigenstates of the radical and compare our vibronic level assignments with the available spectroscopic data from the absorption spectra.

The paper is organized as follows. Section II provides the technical and numerical details of the vibrational and vibronic level computations. Results of the numerical simulations are given, analyzed, and discussed in detail in Section III and the conclusions of this work are summarized in Section IV.

II. COMPUTATIONAL DETAILS

The powerful multi-configuration time dependent Hartree (MCTDH) approach,[75,76] suitable for the representation of wave functions of large systems, is used to tackle the vibrational and vibronic problems of the NO_3^- and NO_3 tetra-atomic systems. The state average and block diagonalisation scheme as described in Ref. 77 are used to compute NO_3^- vibrational and NO_3 vibronic levels. The potential operator of the Hamiltonian is given by the single NO_3^- surface or by the diabatic 2×2 potential matrix for the radical, respectively. Both PES models have been described in detail in our previous work.[55] Some key features of the PESs of the NO_3 radical are provided in the supplementary material. Two kinetic energy operators, *id est* two sets of coordinates, have been used. The first set consists of the six internal stereographic coordinates introduced in Ref. 78, which leads to an optimal expression for the exact kinetic energy operator. The north pole projection version of the three radial $r_1^{(st)}, r_2^{(st)}, r_3^{(st)}$, the angular $\theta^{(st)}$, and the two orientational $s_3^{(st)}, t_3^{(st)}$ stereographic coordinates is employed as detailed in Ref. 79. In this coordinate set, planarity corresponds to $t_3^{(st)} = 0$. The corresponding kinetic energy term for a non-rotating NO_3^- or NO_3 given in Ref. 79 respects the sum of products of single particle operators constraint imposed by MCTDH to allow for a numerically efficient evaluation of operators. The second set consists of the six internal curvilinear coordinates as proposed in Ref. 80. These six internal curvilinear coordinates $\rho^{(cu)}, \vartheta^{(cu)}, \varphi^{(cu)}, \theta^{(cu)}, \phi^{(cu)}, \chi^{(cu)}$ are based on the three Radau vectors of the AB_3 system. Though not all the actual coordinates can be visualised directly, Fig. 1 gives a schematic view of the Radau vectors as well as the three angles $\theta^{(cu)}, \phi^{(cu)}$, and $\chi^{(cu)}$. Planarity is given for $\theta^{(cu)} = \pi/2$, where $\theta^{(cu)}$ is defined as the angle between each of the Radau vectors and the trisector of the Radau vectors. The corresponding quantum mechanical kinetic energy operator[80] contains a non-factorizable term in the MCTDH sense that is approximated by a fourth order Taylor expansion as given in Ref. 47. This quasi-exact kinetic energy operator yielded accurate results when tested in calculations of CH_3 vibrational eigenstates as well as for the NO_3^- first few vibrational levels.[55]

The reason for the introduction of the second curvilinear coordinate set is twofold. First we expect that for the eigenvector representations, the correlation between the coordinates is less pronounced than with the stereographic coordinates due to the more physical nature of these coordinates. The consequence is a faster convergence of the MCTDH scheme with respect to the number of single particle functions. Second and most importantly, when using this second set of coordinates, one can easily evaluate the effect of the symmetry operators of the C_{2v} subgroup of the relevant D_{3h} symmetry group. With the xy plane being the molecular plane, see Fig. 1, the σ_{xy} reflexion acts on the $\theta^{(cu)}$ only around the $\pi/2$ symmetry point, the σ_{xz}

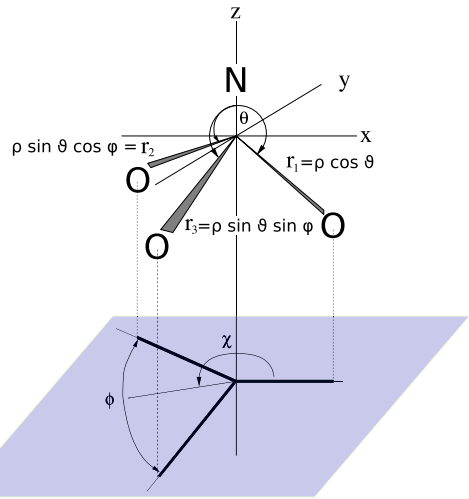

FIG. 1. Representation of the four atoms of NO_3/NO_3^- and of the three Radau vectors in the xyz axis frame together with the 3 angular internal curvilinear coordinates (the subscript (cu) has been dropped in the figure for readability). $\rho^{(cu)}, \vartheta^{(cu)}$, and $\varphi^{(cu)}$ (not depicted here) correspond to the transformation of the three Radau lengths r_1, r_2, r_3 in the hyperspherical representation as given by the formulas.

TABLE I. Wave function representations given by the number of single particle functions (n), the number of Fourier points (N), and the range of the underlying box [in a.u.] for the six stereographic coordinates constructed using mass weighted Cartesian coordinates for both NO_3^- and NO_3.

	NO_3^-			NO_3		
Coordinates	n	N	Range	n	N	Range
$r_1^{(st)}$	9	48	[352 : 522]	8	48	[348 : 522]
$r_2^{(st)}$	9	48	[352 : 522]	8	48	[348 : 522]
$r_3^{(st)}$	9	48	[352 : 522]	8	48	[348 : 522]
$\theta^{(st)}$	11	32	[1.80 : 2.40]	10	32	[1.78 : 2.45]
$s_3^{(st)}$	11	32	[−0.76 : −0.36]	10	32	[−0.806 : −0.368]
$t_3^{(st)}$	8	32	[−0.17 : 0.17]	8	32	[−0.25 : 0.25]
Electronic	1	1		2	2	

reflexion acts on both $\varphi^{(cu)}$ and $\chi^{(cu)}$ around the $\pi/4$ and the π symmetry points, respectively, and the C_2 rotation acts on the three $\theta^{(cu)}$, $\varphi^{(cu)}$, and $\chi^{(cu)}$ angles. The use of two sets of coordinates also is a stringent test of the numerical accuracy of the energy levels. And the computation with the stereographic set ensures that exact energy levels are computed since the kinetic operator has no approximation in this case.

Although the kinetic energy terms fulfill the sum of products of the single particle constraint of MCTDH friendly operators, the potential term does not respect this requirement. Therefore, for the anion, the evaluation of the single-state (or single-valued) potential term is carried out using the original correlation discrete variable representation (CDVR) scheme.[81] The generalized version of CDVR as detailed in the appendix of Ref. 46 is employed for the evaluation of the diabatic two by two potential matrix of the radical.

Tables I and II give the basis set details for both sets of coordinates and both systems. The box range, underlying grid size N, and number of single particle functions n have been carefully converged to ensure the numerical accuracy of the final results to be better than the wave-number for each case.

The labelling of the eigenstates of NO_3^- and NO_3 as excitations in the 6 vibrational modes is not trivial except for the low energy part of the spectrum. Both systems are represented by D_{3h} symmetric PESs and thus the eigenstates have to transform like irreducible representations (irreps) of the D_{3h} point group. Unfortunately, only C_{2v} irreps could be computed from

TABLE II. Wave function representations given by the number of single particle functions (n), the number of Fourier points (N), and the range of the underlying box [in a.u.] for the six curvilinear coordinates constructed using mass weighted Cartesian coordinates for both NO_3^- and NO_3.

	NO_3^-			NO_3		
Coordinates	n	N	Range	n	N	Range
$\rho^{(cu)}$	6	32	[640 : 800]	7	32	[640 : 800]
$\vartheta^{(cu)}$	7	32	[0.805 : 1.105]	10	32	[0.805 : 1.105]
$\varphi^{(cu)}$	7	32	[0.615 : 0.955]	11	32	[0.615 : 0.955]
$\theta^{(cu)}$	6	32	[1.431 : 1.711]	7	32	[1.431 : 1.711]
$\phi^{(cu)}$	8	32	[0.860 : 1.235]	9	32	[0.860 : 1.235]
$\chi^{(cu)}$	8	32	[2.829 : 3.454]	9	32	[2.829 : 3.454]
Electronic	1	1		2	2	

TABLE III. Relation between irreps in C_{2v} and D_{3h} within the orientational convention of this work. The characters with respect to the two σ_v reflexions of C_{2v} are also provided for convenience.

$\Gamma_{D_{3h}}$	$\Gamma_{C_{2v}}$	$\sigma_v(xy)$	$\sigma_v(xz)$
a_1' or e'	a_1	1	1
a_2' or e'	b_1	1	−1
a_1'' or e''	a_2	−1	−1
a_2'' or e''	b_2	−1	1

the MCTDH wave packets. The irreps $\Gamma_{C_{2v}}$ of the eigenfunctions alone, given in Table III, are insufficient to determine the symmetry irrep in D_{3h}. Either one of the two σ_v of the C_{2v} group can be matched to the σ_h of the D_{3h}. The convention used in this work is the natural one when coming from the D_{3h} view point where the C_3 rotational axis is aligned along z. For standard C_{2v}, this is the less common convention and therefore we clearly indicate in the table the nature and characters with respect to the reflections σ_v. In principle, from both the energy degeneracy and $\Gamma_{C_{2v}}$ of the eigenfunctions, $\Gamma_{D_{3h}}$ could be deduced. However, accidental degeneracies and numerical errors pose a problem for the unequivocal symmetry assignments. Moreover, the distinction between the 6 modes is not possible from $\Gamma_{D_{3h}}$ alone. Visual checks of two-dimensional projections of the eigenfunctions are definitely of valuable help but are still insufficient, especially for the assignment of higher excitations. A complimentary way of computing the energy levels for NO_3^- is thus used. A time-independent Hermite discrete variable representation (DVR) approach is utilized[82] and the corresponding Hamiltonian is diagonalized by an exact short iterative Lanczos method. Normal coordinates of the undistorted NO_3^- are used and vibrational angular momenta are ignored in the kinetic energy operator. Standard harmonic oscillator functions are chosen for the finite basis representation (FBR) and the kinetic energy is transformed into the corresponding DVR grid point basis. The six coordinates and their irreps in D_{3h} correspond to totally symmetric stretch (ν_1, a_1'), out-of-plane or umbrella bending (ν_2, a_2''), asymmetric stretch (ν_{3x}/ν_{3y}, e'), and asymmetric bend (ν_{4x}/ν_{4y}, e'), respectively. The associated numbers of basis functions/DVR grid points are 21, 19, 18, 18, 20, and 20, which yield total energies converged to better than 10^{-1} cm^{-1} when compared to a basis with one basis function less in each mode. The degeneracies are reproduced to better than 10^{-2} cm^{-1} for all degenerate levels. The diagonalization is carried out in the DVR basis and the resulting eigenvectors are transformed back into the FBR, in which the eigenstate composition can be analyzed conveniently in terms of vibrational quanta in each of the modes.

We could not compute the radical eigenstates using the DVR method because the basis size required is far beyond our computational capacity and the limitations of our code. However, the possibility to solve the vibrational problem of the anion by both DVR and MCTDH methods was instrumental for the analysis of the vibronic eigenstates of the radical obtained by MCTDH. First, the DVR and MCTDH results of the anion vibrational eigenstates were calculated in excellent agreement. Since the DVR results can be assigned without any

ambiguity, we know the assignment of the MCTDH eigenstates for the anion as well. Due to the coordinate systems used in the MCTDH calculations, the corresponding eigenstates do not show simple nodal structures and thus are not easy to interpret. But since we know the assignments for the anion, certain structures of the eigenstates could be identified and used for the interpretation of the radical eigenstates. This is still not sufficient for a solid assignment but gives valuable additional evidence. This is particularly important since the much more demanding calculations for the radical yield larger energy deviations from the perfect degeneracies of e' and e'' states. Together with the very high density of states, this hampers an unambiguous assignment of degenerate states. The other important piece of evidence besides the comparison to anion states is a simple theoretical model predicting the level structure and accounting for tunneling and the geometric phase. This model will be outlined below.

III. RESULTS AND DISCUSSION

In the following, we first present and discuss the vibrational eigenstates of the NO_3^- anion, which represents the common case of an electronic ground state with a typical single-sheeted PES. This way we obtain a detailed insight into the symmetry properties of the eigenstates for such a prototypical D_{3h} molecule. The results are also compared with the previous findings for the NO_3 radical ground state.[61,62] The situation for the excited $^2E''$ electronic state of the radical is very different due to the Jahn-Teller effect so that two coupled PESs have to be accounted for. The consequences of this vibronic coupling and the resulting geometric phase effect are rationalized by a simple model, which then is utilized to analyze the computed eigenstates. The state assignments following from this analysis finally are used to compare our theoretical results with the available spectroscopic data.

A. Vibrational eigenstates in the NO_3^- $^1A_1'$ electronic state

The 41 first energy levels for the anion, corresponding to the lowest 61 eigenstates, are gathered in Table IV. The MCTDH energies obtained using either the stereographic or the curvilinear coordinates are the same to better than one wave-number for the reported 61 energies. The details of the basis sets are given in Tables I and II. For each calculation, the number of iterations of the MCTDH scheme has been optimized to ensure converged energies again better than one wave-number. The automatic symmetry analysis in C_{2v} of the corresponding eigenfunctions and the degeneracy of the levels help to obtain the corresponding D_{3h} symmetry assignments (fourth column of Table IV). The correct degeneracies are reproduced by the MCTDH calculations to within 10^{-1} cm^{-1} and by the DVR calculation to better than 10^{-2} cm^{-1}. For the lower energy range, this is sufficient to clearly assign a vibrational mode excitation to each level. When the excitation energy is high enough to get double excitations in the asymmetric degenerate ν_3 and ν_4 modes, the time-independent DVR computation based on the exact diagonalization of the vibrational Hamiltonian, for which a clear expansion in vibrational harmonic oscillator functions is obtained, is crucial to get the proper assignments. The symmetry labels and expected energy levels for higher excitations in the degenerate modes and combination bands involving them can be deduced from the proper application of group theory and combinatorics.

The assignments for the fundamentals, energy levels 1 to 4, are straightforward. Energy levels 5 and 6 both correspond to two vibrational quanta in the degenerate bending mode, ν_4. The two quanta can be distributed over the two state components x, y in exactly three ways (x^2, y^2, and xy), which form a reducible representation of the D_{3h} group. This is decomposed into the irreducible representations a_1' and e', in agreement with the assignment based on the automatic C_{2v} symmetry analysis of the wave function. The detailed state compositions in terms of the harmonic oscillator functions obtained by the time-independent DVR calculation are given in the sixth column of Table IV. The v_α^i correspond to the ith harmonic oscillator function in mode α. Note that we omit the normalization of the linear combinations given in Table IV for the sake of a compact representation. The proper linear combinations are deduced from the analysis of the actual Hartree products of harmonic oscillator functions and comparison with the known symmetry polynomials of coordinates. For the D_{3h} point group, the latter can be found, e.g., in our previous work.[42,55] The assignment of levels 7 to 10 is straightforward again because these states correspond to various combination bands or higher excitations involving at most one quantum in an e' mode. By contrast, states 11 to 13 result from the two quanta combinations of the two e' modes, for which four different configurations exist. The eigenstates corresponding to irreps a_1' and e' are equivalent to the second order terms $v_{ee}^{(2,1)}$, $w_{ee}^{(2,1)}$, and $z_{ee}^{(2,1)}$, respectively, as given in the appendix of Ref. 55. The eigenstate corresponding to a_2' can be obtained simply by orthogonality arguments. State 14 again is straightforward and results from the double excitation of the totally symmetric stretching mode ν_1. The next three eigenstates belong to the manifold of triple excitations in the e' asymmetric bending mode, ν_4, for which four configurations exist. The a_1' state composition, belonging to state 17, corresponds to the $\mathcal{V}^{(3)}$ potential term as given in Ref. 42. Note, however, that due to the normalization factors of the harmonic oscillator functions a factor of $\sqrt{3}$ rather than a factor of 3 arises. State 16 is the a_2' counterpart to state 17 and its composition is easily obtained by exchanging the roles of x and y components with respect to the a_1' state. Finally, state 15 transforms like e' as expected and the compositions of the two state components can be found either by orthogonality or by combining the Hartree products to yield the $\mathcal{W}^{(3)}/\mathcal{Z}^{(3)}$ symmetry polynomials of Ref. 42, respectively. The next energy levels, 18 to 29 are various combination bands or higher excitations for which the wave functions can be explained in terms of the already discussed states. The next interesting manifold of states originates from the configuration $3^1 4^2$, a higher combination mode of the two e' vibrations. The six possible configurations lead to two e' states, one a_1', and one a_2' state, respectively. The expansion coefficients for the symmetrized Hartree product transforming like a_1' are obtained by reproducing the symmetrized polynomial $v_{ee}^{(3,1)}$ of Ref. 55. The a_2' function simply

TABLE IV. Vibrational eigenstates of NO_3^-, zero-point, and excitation energies in cm^{-1}, level symmetries in C_{2v} and D_{3h}, and state assignments including dominant state contributions.

i	E_0 or $E_i - E_0$	$\Gamma_{C_{2v}}$	$\Gamma_{D_{3h}}$	Assignment	Composition
0	3038.8	a_1	a_1'	0	
1	702.5/702.5	b_1/a_1	e'	4^1	ν_{4y}^1/ν_{4x}^1
2	843.7	b_2	a_2''	2^1	ν_2^1
3	1040.1	a_1	a_1'	1^1	ν_1^1
4	1352.9/1352.9	a_1/b_1	e'	3^1	ν_{3x}^1/ν_{3y}^1
5	1403.2	a_1	a_1'	4^2	$\nu_{4y}^2+\nu_{4x}^2$
6	1405.3/1405.3	b_1/a_1	e'		$\nu_{4y}^1\nu_{4x}^1/\nu_{4y}^2-\nu_{4x}^2$
7	1544.4/1544.4	a_2/b_2	e''	2^14^1	$\nu_2^1\nu_{4y}^1/\nu_2^1\nu_{4x}^1$
8	1683.8	a_1	a_1'	2^2	ν_2^2
9	1740.4/1740.4	a_1/b_1	e'	1^14^1	$\nu_1^1\nu_{4x}^1/\nu_1^1\nu_{4y}^1$
10	1880.5	b_2	a_2''	1^12^1	$\nu_1^1\nu_2^2$
11	2046.6	b_1	a_2'	3^14^1	$\nu_{3x}^1\nu_{4y}^1-\nu_{3y}^1\nu_{4x}^1$
12	2048.4/2048.4	b_1/a_1	e'		$\nu_{3x}^1\nu_{4y}^1+\nu_{3y}^1\nu_{4x}^1/\nu_{3x}^1\nu_{4x}^1-\nu_{3y}^1\nu_{4y}^1$
13	2049.2	a_1	a_1'		$\nu_{3x}^1\nu_{4x}^1+\nu_{3y}^1\nu_{4y}^1$
14	2077.6	a_1	a_1'	1^2	ν_1^2
15	2103.9/2103.9	b_1/a_1	e'	4^3	$\sqrt{3}\nu_{4y}^3+\nu_{4x}^2\nu_{4y}^1/\sqrt{3}\nu_{4x}^3+\nu_{4x}^1\nu_{4y}^2$
16	2107.8	b_1	a_2'		$\nu_{4y}^3-\sqrt{3}\nu_{4x}^2\nu_{4y}^1$
17	2108.4	a_1	a_1'		$\nu_{4x}^3-\sqrt{3}\nu_{4x}^1\nu_{4y}^2$
18	2190.5/2190.5	b_2/a_2	e''	2^13^1	$\nu_2^1\nu_{3x}^1/\nu_2^1\nu_{3y}^1$
19	2243.2	b_2	a_2''	2^14^2	$\nu_2^1\nu_{4x}^2+\nu_2^1\nu_{4y}^2$
20	2245.3/2245.3	a_2/b_2	e''		$\nu_2^1\nu_{4x}\nu_{4y}^1/\nu_2^1\nu_{4x}^2-\nu_2^1\nu_{4y}^2$
21	2380.2/2380.2	a_1/b_1	e'	1^13^1	$\nu_1^1\nu_{3x}^1/\nu_1^1\nu_{3y}^1$
22	2382.8/2382.8	b_1/a_1	e'	2^24^1	$\nu_2^2\nu_{4y}^1/\nu_2^2\nu_{4x}^1$
23	2438.7	a_1	a_1'	1^14^2	$\nu_1^1\nu_{4x}^2+\nu_1^1\nu_{4y}^2$
24	2440.3/2440.3	b_1/a_1	e'		$\nu_1^1\nu_{4x}^1\nu_{4y}^1/\nu_1^1(\nu_{4x}^2-\nu_{4y}^2)$
25	2520.6	b_2	a_2''	2^3	ν_2^3
26	2579.0/2579.0	b_2/a_2	e''	$1^12^14^1$	$\nu_1^1\nu_2^1\nu_{4x}^1/\nu_1^1\nu_2^1\nu_{4y}^1$
27	2679.7	a_1	a_1'	3^2	$\nu_{3y}^2+\nu_{3x}^2$
28	2704.6/2704.6	b_1/a_1	e'		$\nu_{3y}^1\nu_{3x}^1/\nu_{3y}^2-\nu_{3x}^2$
29	2717.5	a_1	a_1'	1^12^2	$\nu_1^1\nu_2^2$
30	2740.7/2740.7	b_1/a_1	e'	3^14^2	$\nu_{3y}^1(\nu_{4y}^2+\nu_{4x}^2)/\nu_{3x}^1(\nu_{4x}^2+\nu_{4y}^2)$
31	2743.6	a_1	a_1'		$\nu_{3x}^1\nu_{4x}^2-\nu_{3x}^1\nu_{4y}^2-\sqrt{2}\nu_{3y}^1\nu_{4x}^1\nu_{4y}^1$
32	2743.9	b_1	a_2'		$\nu_{3y}^1\nu_{4y}^2-\nu_{3y}^1\nu_{4x}^2-\sqrt{2}\nu_{3x}^1\nu_{4x}^1\nu_{4y}^1$
33	2745.5/2745.5	a_1/b_1	e'		$\nu_{3x}^1(\nu_{4x}^2-\nu_{4y}^2)+\sqrt{2}\nu_{3y}^1\nu_{4x}^1\nu_{4y}^1/\nu_{3y}^1(\nu_{4y}^2-\nu_{4x}^2)+\sqrt{2}\nu_{3x}^1\nu_{4x}^1\nu_{4y}^1$
34	2776.1/2776.1	a_1/b_1	e'	1^24^1	$\nu_1^2\nu_{4x}^1/\nu_1^2\nu_{4y}^1$
35	2802.8	a_1	a_1'	4^4	$\nu_{4x}^4+\sqrt{\frac{2}{3}}\nu_{4x}^2\nu_{4y}^2+\nu_{4y}^4$
36	2804.7/2804.8	b_1/a_1	e'		$\nu_{4x}^3\nu_{4y}^1+\nu_{4x}^1\nu_{4y}^3/\nu_{4x}^4-\nu_{4y}^4$
37	2810.8/2810.8	b_1/a_1	e'		$\nu_{4x}^3\nu_{4y}^1-\nu_{4x}^1\nu_{4y}^3/\nu_{4x}^4-\sqrt{6}\nu_{4x}^2\nu_{4y}^2+\nu_{4y}^4$
38	2882.4	a_2	a_1''	$2^13^14^1$	$\nu_2^1(\nu_{3x}^1\nu_{4y}^1-\nu_{3y}^1\nu_{4x}^1)$
39	2884.2/2884.2	a_2/b_2	e''		$\nu_2^1(\nu_{3x}^1\nu_{4y}^1+\nu_{3y}^1\nu_{4x}^1)/\nu_2^1(\nu_{3x}^1\nu_{4x}^1-\nu_{3y}^1\nu_{4y}^1)$
40	2885.1	b_2	a_2''		$\nu_2^1(\nu_{3x}^1\nu_{4x}^1+\nu_{3y}^1\nu_{4y}^1)$

results from exchanging the x and y components of the a_1' basis function. The two different e_x' symmetry functions are found by correspondence to the two different polynomials $w_{ee}^{(3,2)}$ and $w_{ee}^{(3,4)}$, and the e_y' basis functions arise from exchanging the x and y components or by using the polynomials $z_{ee}^{(3,2)}$ and $z_{ee}^{(3,4)}$. The computed eigenstates of e' symmetry both show a significant mixture of the two pairs of symmetrized basis functions listed in the table. State 30 (re-normalized in the subspace of

the two basis functions) shows coefficients of roughly 0.84 and −0.54 and state 33 is the orthogonal counter part. State 34 arises from a double excitation of the totally symmetric stretching mode and one quantum in ν_4, thus transforming as e'. The next set of states (35-37) belongs to quadruple excitations in ν_4 for which five distinct configurations exist for the distribution of four vibrational quanta over two mode components. This results in one a_1' state and two e' states, and the symmetrized Hartree products are found in analogy to the previously discussed states from the symmetry polynomials $\mathcal{V}^{(4)}$, $\mathcal{W}^{(4,1)}/\mathcal{Z}^{(4,1)}$, and $\mathcal{W}^{(4,2)}/\mathcal{Z}^{(4,2)}$, respectively. In this case, the compositions of the computed e' eigenstates (states 35 and 36) show hardly any mixing of the two sets of e' basis functions in contrast to states 30 and 33. The last three states of our computations, 38-40, arise from a three mode combination band with one quantum each in the umbrella, the asymmetric stretch, and the asymmetric bending mode. This results in states transforming as a_1'', a_2'', and e'', and the symmetry functions can be easily obtained from the results already discussed above.

Our results for the anion can be compared to the calculations of Stanton for the ground state of the radical.[61] This latter state of $^2A_2'$ symmetry also has a single-sheeted PES with a D_{3h} symmetric equilibrium geometry like the anion. For both systems, the lowest excitation is found for 4^1 but the striking difference is that the frequency in the case of the anion is almost twice that of the radical. Thus, the next levels in the radical were found to be due to 4^2. We observe a fairly harmonic progression for this state in the case of the anion with a small splitting of 2.1 cm^{-1} between the a_1' and e' levels, while the radical shows a strong negative anharmonicity and a larger splitting of 5.5 cm^{-1} for this set of states. The frequency for the 1^1 level is about 11 cm^{-1} lower for the anion but the frequency for the 3^1 asymmetric stretching excitations is almost 360 cm^{-1} lower for the radical. The latter is a very much disputed number for the radical due to a controversy about the interpretation of experimental results. It appears that the radical in its electronic ground state is much more easily deformed asymmetrically than the anion, which has been explained by the strong *pseudo*-Jahn-Teller coupling to the second excited electronic state of $^2E'$ symmetry. We note that the sets of states arising from the same excitation configurations, like the three states corresponding to 4^3, are in perfect agreement between the radical and anion calculations. A striking difference is, however, that the splittings between levels of the same set are significantly larger in the case of the radical. There is only one exception, namely, the 3^2 manifold, for which the splitting in the radical is less than half that of the corresponding anion state. This state manifold also indicates a slightly negative anharmonicity in the case of the radical while a slightly positive anharmonicity is found for the anion. In the light of the new anion results, the radical ground state seems to behave rather unusual and is certainly worth to be revisited with a more sophisticated model in the future.

B. Vibronic eigenstates in the $^2E''$ electronic state

We now turn our attention to the $^2E''$ first excited state of the NO_3 radical. The global symmetry of the two coupled PESs for the electronic state is D_{3h} and thus the vibronic eigenstates have to show the same fundamental properties as those presented for the anion. However, the fairly strong Jahn-Teller effect in this state leads to a much more complicated situation as will be discussed below. Unfortunately, the eigenstates could not be determined by the time-independent DVR method. Therefore, the lowest vibronic energy levels for the neutral NO_3 radical are only computed by the MCTDH method and are gathered in Table V. The table presents 45 energies, obtained using each of the two coordinate sets, as well as the C_{2v} irreducible representation of the corresponding eigenvectors. The comparison between the two sets of computed energy values emphasizes the good numerical accuracy of the energies reported. Furthermore, two sets of tentative assignments of the vibronic symmetry labels in D_{3h} are given.

When compared with the anion, a much more congested spectrum is obtained for the radical with 36 levels below 1400 cm^{-1} of the excitation energy for NO_3 and only 6 for NO_3^-. These numbers also can be compared with NO_3 in the $^2A_2'$ ground electronic state for which 12 levels are found below 1400 cm^{-1} of the excitation energy.[61] This higher density of states is in part due to the triple well shape of the lower adiabatic PES sheet of this state and to the two intersecting electronic surfaces for the radical. Due to the multi-sheeted potential surface, the calculations are computationally much more demanding than for the single D_{3h} centered well of the anion. A consequence is a somewhat less accurate representation of the degeneracies as obvious already for the ground vibronic state. We also were not able to use the time-independent DVR method to compute the eigenstates and thus are much more limited in the analysis of the eigenstates. The labelling of the D_{3h} irreps is not obvious due to the combination of the density of states and of the intrinsic complexity of the spectrum as discussed below.

C. Tunnelling and geometric phase effect in the $^2E''$ electronic state

The PESs for the $^2E''$ state of NO_3 show some intriguing features that are responsible for the complex and somewhat enigmatic spectra. The lower adiabatic PES has three equivalent and fairly pronounced minima due to the Jahn-Teller effect, which are connected by rather low barriers to *pseudo*-rotation. The barrier heights are only 1250.9 cm^{-1}, which is less than, e.g., the height of the barrier to inversion of ammonia (1766–1777 cm^{-1}).[83,84] In the absence of spin-orbit coupling, there is a two-dimensional intersection seam with the upper adiabatic PES spanned by the nuclear coordinates of a_1' and a_2'' symmetries and thus not lifting the D_{3h} symmetry of the system. The minimum of the seam of crossing is found 2850.6 cm^{-1} above the minima for a planar geometry with N–O distances of 2.3860 bohrs compared to the equilibrium distance on the ground state PES of 2.3444 bohrs for which an energy of 3217.7 cm^{-1} above the minima is found. We computed the spin-orbit splitting at the equilibrium geometry of the electronic ground state to be about 1 cm^{-1} for the $^2E''$ state, which is too small to lift the degeneracy effectively and thus can be neglected for the present study. Each point on the seam corresponds to a conical intersection with respect to

TABLE V. Excitation energies in cm^{-1} for NO_3 above the ground state $E_0^{(st)} = 2732.11\ cm^{-1}$ and $E_0^{(cu)} = 2732.13\ cm^{-1}$ obtained with stereographic (st) and curvilinear (cu) coordinates. $\Gamma_{C_{2v}}$ is the irreducible representation obtained from the symmetry analysis of the eigenfunctions when using the curvilinear coordinates. For each assigned level, the corresponding D_{3h} label together with the corresponding mode excitations are provided in bold face. The other labels given in the "key" and the "assignment" columns correspond to tentative assignment (see text for discussion).

Key	$(E_i - E_0)^{(st)}$	$(E_i - E_0)^{(cu)}$	$\Gamma_{C_{2v}}$	Assignment	
1_α	0.00	0.00	a_2	$e''\ \mathbf{0}(a_1)$	$e''\ \mathbf{0}(a_1)$
1_β	0.16	0.14	b_2	$e''\ \mathbf{0}(a_1)$	$e''\ \mathbf{0}(a_1)$
1_γ	52.92	52.91	b_2	$a_2''\ \mathbf{0}(a_1)$	$a_2''\ \mathbf{0}(a_1)$
2_α	549.09	549.07	a_2	$a_1''\ \mathbf{4^1}(b_1)$	$a_1''\ \mathbf{4^1}(b_1)$
2_β	580.42	580.41	b_2	$e''\ \mathbf{4^1}(b_1)$	$e''\ \mathbf{4^1}(a_1)$
2_γ	580.82	580.80	a_2	$e''\ \mathbf{4^1}(b_1)$	$e''\ \mathbf{4^1}(a_1)$
3_α	602.22	602.23	b_1	$e'\ \mathbf{2^1}(b_2)$	$e'\ \mathbf{2^1}(b_2)$
3_β	602.41	602.39	a_1	$e'\ \mathbf{2^1}(b_2)$	$e'\ \mathbf{2^1}(b_2)$
3_γ	642.63	642.63	a_1	$a_1'\ \mathbf{2^1}(b_2)$	$a_1'\ \mathbf{2^1}(b_2)$
4_α	642.83	642.84	b_2	$a_2''\ \mathbf{4^1}(a_1)$	$a_2''\ \mathbf{4^1}(a_1)$
4_β	653.84	653.85	a_2	$e''\ \mathbf{4^1}(a_1)$	$e''\ \mathbf{4^1}(b_1)$
4_γ	654.39	654.38	b_2	$e''\ \mathbf{4^1}(a_1)$	$e''\ \mathbf{4^1}(b_1)$
5_α	809.47	809.49	a_2	$e''\ \mathbf{1^1}(a_1)$	$e''\ \mathbf{1^1}(a_1)$
5_β	809.84	809.83	b_2	$e''\ \mathbf{1^1}(a_1)$	$e''\ \mathbf{1^1}(a_1)$
5_γ	929.88	929.89	b_2	$a_2''\ \mathbf{1^1}(a_1)$	$a_2''\ \mathbf{1^1}(a_1)$
9_α	1111.27	1111.22	b_2	$e''\ 4^2(a_1)$	$e''\ 4^2(a_1)$
9_β	1111.76	1111.74	a_2	$e''\ 4^2(a_1)$	$e''\ 4^2(a_1)$
10_α	1136.94	1136.96	a_2	$a_1''\ 4^2(b_1)$	$a_1''\ 4^2(b_1)$
6_α	1156.49	1156.46	b_1	$a_2'\ \mathbf{2^1 4^1}(a_2)$	$a_2'\ \mathbf{2^1 4^1}(a_2)$
10_β	1159.65	1159.64	a_2	$e''\ 4^2(b_1)$	$e''\ 4^2(b_1)$
10_γ	1159.86	1159.83	b_2	$e''\ 4^2(b_1)$	$e''\ 4^2(b_1)$
9_γ	1164.59	1164.54	b_2	$a_2''\ 4^2(a_1)$	$a_2''\ 4^2(a_1)$
6_β	1177.69	1177.69	a_1	$e'\ \mathbf{2^1 4^1}(a_2)$	$e'\ \mathbf{2^1 4^1}(a_2)$
6_γ	1178.22	1178.20	b_1	$e'\ \mathbf{2^1 4^1}(a_2)$	$e'\ \mathbf{2^1 4^1}(a_2)$
11_α	1229.34	1229.32	a_2	$e''\ 2^2(a_1)$	$e''\ 2^2(a_1)$
11_β	1229.66	1229.71	b_2	$e''\ 2^2(a_1)$	$e''\ 2^2(a_1)$
7_α	1236.98	1237.00	b_1	$e'\ \mathbf{2^1 4^1}(b_2)$	$e'\ \mathbf{2^1 4^1}(b_2)$
11_γ	1237.09	1237.06	b_2	$a_2''\ 2^2(a_1)$	$a_2''\ 2^2(a_1)$
7_β	1237.74	1237.74	a_1	$e'\ \mathbf{2^1 4^1}(b_2)$	$e'\ \mathbf{2^1 4^1}(b_2)$
7_γ	1243.70	1243.72	a_1	$a_1'\ \mathbf{2^1 4^1}(b_2)$	$a_1'\ \mathbf{2^1 4^1}(b_2)$
12_α	1250.25	1250.30	a_2	$e''\ 4^2(a_1) \circ$	$e''\ 3^1(a_1)$
12_β	1250.44	1250.47	b_2	$e''\ 4^2(a_1) \circ$	$e''\ 3^1(a_1)$
13_α	1270.23	1270.24	a_2	$e''\ 3^1(a_1)$	$e''\ 1^1 4^1(a_1)$
13_β	1270.32	1270.31	b_2	$e''\ 3^1(a_1)$	$e''\ 1^1 4^1(a_1)$
12_γ	1274.84	1274.93	b_2	$a_2''\ 4^2(a_1) \circ$	$a_2''\ 3^1(a_1)$
14_α	1300.06	1300.04	a_2	$a_1''\ 1^1 4^1(b_1)$	$a_1''\ 3^1(b_1)$
13_γ	1366.27	1366.26	b_2	$a_2''\ 3^1(a_1)$	$a_2''\ 1^1 4^1(a_1)$
8_α	1407.28	1407.33	b_1	$e'\ \mathbf{1^1 2^1}(b_2)$	$e'\ \mathbf{1^1 2^1}(b_2)$
8_β	1407.54	1407.54	a_1	$e'\ \mathbf{1^1 2^1}(b_2)$	$e'\ \mathbf{1^1 2^1}(b_2)$
14_β	1407.66	1407.65	b_2	$e''\ 1^1 4^1(b_1)$	$e''\ 3^1(b_1)$
14_γ	1407.98	1407.93	a_2	$e''\ 1^1 4^1(b_1)$	$e''\ 3^1(b_1)$
15_α	1465.78	1465.77	a_2	$a_1''\ 3^1(b_1)$	$a_1''\ 1^1 4^1(b_1)$
15_β	1481.52	1481.57	a_2	$e''\ 3^1(b_1)$	$e''\ 1^1 4^1(b_1)$
15_γ	1482.62	1482.63	b_2	$e''\ 3^1(b_1)$	$e''\ 1^1 4^1(b_1)$
8_γ	1495.96	1495.98	a_1	$a_1'\ \mathbf{1^1 2^1}(b_2)$	$a_1'\ \mathbf{1^1 2^1}(b_2)$

the four-dimensional coordinate space of the two e' modes, thus inducing a geometric phase effect (GPE). The vibrational zero-point level at 2732.1 cm^{-1} is found noticeably above the barriers to *pseudo*-rotation but just barely below the minimum of the seam of crossing and the energy of the conical intersection at the equilibrium geometry of the electronic ground state. The vibronic ground state is found to be doubly degenerate and of e'' symmetry. This can be understood by considering the shape of the lower adiabatic PES and will be explained in the following.

Figure 2 displays schematic views of the NO_3^- anion on the single-sheeted ground state PES and of the Jahn-Teller distorted radical on the lower sheet of the $^2E''$ state adiabatic PES. The PES corresponding to the anion's ground state has a single well and the equilibrium geometry thus stays D_{3h} symmetric. By contrast, the Jahn-Teller effect active in the $^2E''$ state of the radical results in the triple-well structure of the lower adiabatic PES depicted in the right panel of Fig. 2. The corresponding three equivalent equilibrium geometries result from distortion along each of the three N–O bonds, respectively, and are also depicted in the figure. The distortion affects the ONO angles as well of course. Though the global symmetry of both PESs obviously obeys the threefold rotational symmetry invariance, this is not true for the isolated distorted configurations in each of the wells. When looking at the system in one well and ignoring the existence of the two equivalent configurations in the other wells, the local environment and nuclear configuration are only C_{2v} symmetric. It turns out that the level structure can be understood in terms of corresponding symmetrized local vibrations and tunnelling among the three equivalent potential wells. Assume an artificial potential with C_{3v} or D_{3h} symmetry and infinitely high barriers between three equivalent wells. It is clear that in this case, we can treat the local vibrations separately. However, since the eigenstates need to transform like an irreducible representation of the symmetry transformation group, which the local solutions do not, we need to symmetrize them. The three local solutions form a basis for a 3-dimensional reducible representation, which can be decomposed into irreducible representations $a \oplus e$. The eigenvalues of the three symmetrized solutions will remain degenerate unless the barrier heights become finite, like in a real system. This means that the local vibrations do interact via tunnelling and thus that the degeneracy is lost. However the global D_{3h} symmetry still imposes that the eigenstates transform as irreducible representations of a and e types leading to the level structure of the resulting spectrum. This can be rationalized quite nicely by a next neighbour model similar to Hückel models.

Assume we have a n-fold symmetry axis and corresponding $\widehat{C}_n$ symmetry operator transforming one local state into the other. After n operations of $\widehat{C}_n$ on any local state, one arrives at the same potential well but the wave function has changed

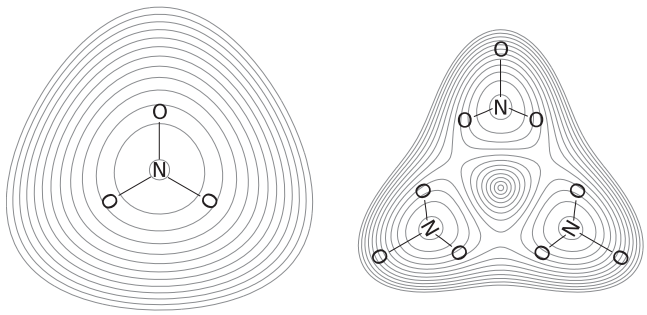

FIG. 2. Pictorial views of the NO_3^- anion (left panel) and distorted NO_3 radical (right panel) geometries superimposed on potential contour plots (NO_3^- ground state on the left and lower adiabatic sheet of the $^2E''$ state on the right).

sign due to the geometric phase effect. If we further assume that the local states can only interfere with the ones in the neighbouring wells, we can write the Schrödinger equation in the next neighbour approximation as

$$\begin{pmatrix} \alpha - E & \beta & 0 & 0 & \dots & \beta^* \\ \beta^* & \alpha - E & \beta & 0 & \dots & 0 \\ 0 & \beta^* & \alpha - E & \beta & \dots & 0 \\ \vdots & & & & \ddots & \vdots \\ \beta & 0 & 0 & \dots & \beta^* & \alpha - E \end{pmatrix} \begin{pmatrix} c_1 \\ c_2 \\ c_3 \\ \vdots \\ c_n \end{pmatrix} = \begin{pmatrix} 0 \\ 0 \\ 0 \\ \vdots \\ 0 \end{pmatrix}. \quad (1)$$

Here α stands for the expectation value of the vibrational Hamiltonian over a purely local eigenstate and β for the overlap integral corresponding to the tunneling interaction with the next neighbour local state. This yields the relation

$$\beta^* c_{j-1} + (\alpha - E) c_j + \beta c_{j+1} = 0, \quad \text{with } 1 < j < n-1, \quad (2)$$

with the restriction of j in Eq. (2) originating from 4π rather than 2π periodicity. One full rotation by 2π around the conical intersection corresponds to n operations of $\widehat{C}_n$ on c_j and the geometric phase requires that $\widehat{C}_n^n c_j = -c_j$ and $\widehat{C}_n^{2n} c_j = c_j$. Thus, there are n solutions for any c_j reading

$$c_j = e^{ijk\pi/n}, \qquad k = 0, 1, \dots n-1. \quad (3)$$

With $\beta = r_\beta e^{i\phi_\beta}$, the solutions of Equation (1) are

$$E_k = \alpha + 2r_\beta \cos\left(\frac{k\pi}{n} + \phi_\beta\right), \qquad k = 0, 1, \dots, n-1. \quad (4)$$

The above symmetry considerations require that

$$\phi_\beta = \sigma_i \nu_i \pi - \frac{(n-1)\pi}{2n}, \quad (5)$$

where σ_i is one if i corresponds to a local vibration that formally would be degenerate and of e_y type in a single-well PES and two for formally non-degenerate or e_x local modes. ν_i is the corresponding vibrational quantum number. σ_i is deduced from the general properties of idealized $E \otimes e$ Jahn-Teller systems for which Ham gave an elegant proof for the sequence of states.[85] Details about this reasoning are given in the supplementary material.

At this point, the relation to the typical perspective from standard idealized vibronic coupling treatments should be pointed out. It is customary to restrict the Jahn-Teller problem to linear and quadratic couplings only and to analyse the vibronic states in terms of coupling strengths. In the absence of quadratic coupling, the adiabatic PESs show cylindrical symmetry and the nuclear dynamics is best interpreted (and treated theoretically) as an angular and a radial motion. All vibronic states can be classified by a corresponding vibronic angular momentum $j = \pm\frac{n}{2}$ ($n = 1, 2 \dots$). In the absence of any vibronic coupling, the problem resumes to the standard 2D isotropic harmonic oscillators for each surface. The states are thus $2(v+1)$-fold degenerate with v being the usual vibrational quantum number. The linear coupling splits levels of different vibronic angular momenta $|j| = \frac{n}{2}$ but does not lift the degeneracy among $j = \pm\frac{n}{2}$ states.[86] When considering the correlation to the D_{3h}/C_{3v} picture, these degenerate pairs transform either as e or as a pair of a_1 and a_2, which are degenerate because the true symmetry of the PES model is higher ($D_{\infty h}/C_{\infty v}$). This is independent of the linear coupling strength, which only increases the depth of the rotationally symmetric moat around the conical intersection point (so-called the Jahn-Teller stabilization energy). As long as the linear coupling is weak, the nuclear dynamics can be interpreted in terms of normal modes corresponding to a geometry with the highest symmetry and the associated vibrational quantum numbers. In our case, this would mean small nuclear oscillations around the D_{3h} symmetric atomic positions. This picture looses validity with increasing linear coupling since the amplitude of the eigenfunctions near the D_{3h} point decreases notably. The dynamics then is best interpreted in terms of an angular motion, characterized by vibronic angular momentum j, and radial oscillations with the associated quantum number v_r. Increasing linear coupling lowers the level energies for higher $|j|$ values, and for strong linear coupling, the first few levels all correspond to excitations in the angular motions while the radial motion is not excited (see the supplementary material and Ref. 86). The quadratic coupling destroys the cylindrical symmetry and leads to multiple equivalent potential wells as discussed above. This also lifts the degeneracy of the pairs transforming as a_1 and a_2. As long as the quadratic coupling is weak and thus the barriers between the equivalent wells are low, an interpretation of the nuclear dynamics as now hindered *pseudo*-rotational (angular) and radial excitation is still reasonable. However, this view looses validity with further increasing quadratic coupling, which leads to deeper wells separated by higher barriers. In such a case, the dynamics is better interpreted as the nuclei carrying out small oscillations around the positions within the local minima of reduced local symmetry.[86] The emergence of this situation (relatively deep wells separated by substantial barriers) has been shown long ago utilizing simple vibronic coupling models. In our three-well case, and for finite quadratic coupling, only the set of half-integer $j \mod 3$ will remain good vibronic quantum numbers. States with $\pm j \mod 3 = \frac{3}{2}$ transform as a_1 or a_2 and are split by the quadratic coupling. This splitting increases with the quadratic coupling strength, and for large quadratic coupling, the a_1 and a_2 levels come close to e levels.[86]

This caused to some confusion in the literature because it can be mistaken as a vibrationally excited state (in the sense of a normal vibration) approaching the ground state level. But in fact, this is the $\left|v_r = 0, j \mod 3 = \frac{3}{2}\right\rangle$ level (a_1 or a_2) coming close to the $\left|v_r = 0, j \mod 3 = \left\{\frac{1}{2}, \frac{5}{2}\right\}\right\rangle$ level (e). This is exactly the situation, which calls for a change of perspective and an interpretation in terms of multiple potential wells and tunnelling as outlined above. Clear evidence for this is given in the supplementary material. This effect is known for the ground state triplet of vibronic states since the 1960s[86] but to the best of our knowledge was hardly discussed for vibrationally excited states. Originally, the impact of the geometric phase effect on the level structure had been unknown. Much later Ham analysed this effect in an elegant way[85] and we use these results in our analysis. As we will show in the following, the situation in the $^2E''$ state of NO_3 is such that both linear and higher order Jahn-Teller couplings are large and that the vibronic eigenstates are most naturally interpreted in terms

of the tunnelling interaction of local vibrations including the geometric phase effect.

The consequences of the adiabatic PES topography and the geometric phase are illustrated by representative examples in the following. We focus first on the vibronic ground state manifold. No vibrational motion of the molecule is excited and thus one would expect the symmetry of the lowest vibrational level to be totally symmetric, a_1' in the case of D_{3h}. This is exactly what is found for the anion ground vibrational state (cf. Table IV). However, in the $^2E''$ state of the radical, the Jahn-Teller effect couples electronic and nuclear motions and thus, strictly speaking, only vibronic states but no vibrational states can be specified because the motions are inseparable. Nevertheless, the level structure of the NO_3 spectrum can be rationalized based on a local separation of electronic and nuclear motions. The Jahn-Teller effect is reflected by the fact that the molecule is distorted resulting in the three equivalent minima of C_{2v} symmetry (see above). Locally in one well, ignoring the existence of the other wells, we can envision the vibrational motions of the molecule as usual and classify them by the local symmetry of C_{2v}. Then the electronic part of the wave function is accounted for in two steps. First, the E character is reflected by the diabatic Hamiltonian, which at first does not distinguish E' and E'' but correctly leads to the triple-well topography of the lower adiabatic PES. In effect, that means that the local vibration needs to be symmetrized according to the C_3 rotation operator of D_{3h}. Second, the anti-symmetry with respect to the reflection on the molecular plane, σ_h, of the electronic part of the wave function is included. One way to visualize this more easily is to use orbitals of appropriate local symmetry to represent the local vibrations. In the current case, one can use an s orbital in a local well corresponding to a_1 in C_{2v} to represent a nodeless vibrational ground state. So, symmetrizing the s orbital with respect to C_3 rotation leads to a set of e' and a_1' orbitals. Second the anti-symmetry with respect to σ_h is included to account for the corresponding symmetry of the $^2E''$ electronic state. This can be achieved by replacing the s orbitals by p_z orbitals yielding e'' and a_2'' vibronic labels. Of course, the order of the two steps is arbitrary and one could also start from the p_z orbital of local b_2 symmetry to include the electronic symmetry with respect to σ_h first and then symmetrize with respect to the C_3 rotation. Finally, due to the geometric phase effect, sets of states corresponding to local non-degenerate vibrations or even quanta in the angular part of a motion correlated to formally an e vibration always have an energy ordering sequence of e below a. By contrast, sets of states corresponding to odd quanta in the angular motion correlated to formally an e vibration are ordered a below e. This effect is displayed schematically in Fig. 3 for the vibronic ground state manifold of the NO_3 $^2E''$ state. This analysis is coherent with the numerical result of a doubly degenerate e'' vibronic ground state and its tunneling pair 52.8 cm^{-1} above (see the three levels $1_{\alpha,\beta,\gamma}$ of Table V).

The same reasoning can be applied to the fundamentals of the system. The symmetric stretch vibration, ν_1, is strictly identical to the ground state case. Such a case is found for the three levels $5_{\alpha,\beta,\gamma}$ of Table V, which therefore we assign to the excitation 1^1. Excitations in the umbrella mode, ν_2, the

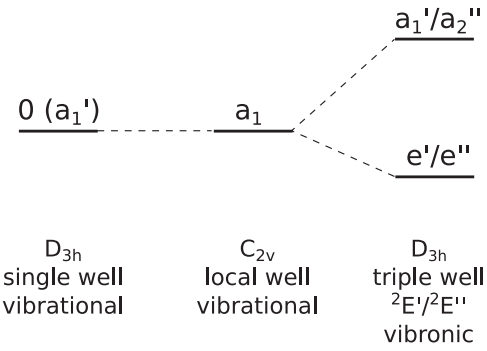

FIG. 3. Schematic level structure of the ground state manifold. Left are state labels according to D_{3h} vibrational modes corresponding to a single-well D_{3h} PES, middle are state labels corresponding to local vibrational modes in one of the three equivalent wells at reduced local symmetry (C_{2v}), right are the correct vibronic levels including tunnelling splitting and GPE in terms of the global D_{3h} symmetry of the PES and specified for an electronic state of E' or E'' symmetry, respectively.

asymmetric bending mode, ν_4, and the asymmetric stretching mode, ν_3, lead to the level structures depicted in Figs. 4–6. Detailed derivations of these results are provided in the supplementary material.

What remains is the analysis of low-lying higher excitations and combination bands of which the first is expected to be the $(\nu_4)^2$ manifold. Since this involves formally degenerate e vibrations of which the degeneracy is lifted by the local C_{2v} symmetry, a more complicated pattern will result. The corresponding scheme is given in Fig. 7.

Finally, we analyze the level structure of supposedly low-lying combination bands. The candidates expected in the range of our computations are $(\nu_2)^1(\nu_4)^1$, $(\nu_1)^1(\nu_4)^1$, and $(\nu_1)^1(\nu_2)^1$. The resulting level schemes are given in Fig. 8 for the three combinations. The mode-mode combination between ν_2 and ν_4 leads to a new pattern not contained in the above examples. The umbrella motion, ν_2 corresponds to a local symmetry of b_2 and combined with the local b_1 symmetry of the presumably lower component of the ν_4 mode in the local well, this results in a_2 local symmetry. This yields vibronic states of a_2' and e' according to our scheme, and since there are odd quanta formally in an e_y mode (ν_4) belonging to angular excitation, the state ordering is a_2' below e'. The upper triplet corresponds to a pure radial excitation and thus is ordered e' below a_1'. By contrast, the corresponding combination of ν_2 with the upper component of local a_1 symmetry of ν_4 yields

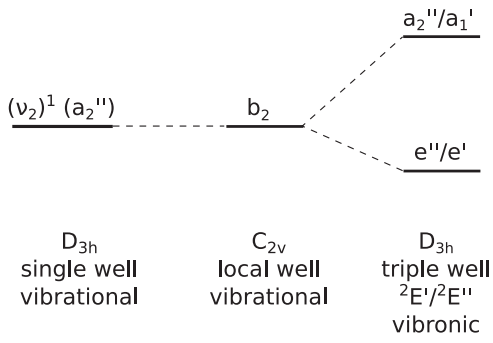

FIG. 4. Schematic level structure corresponding to odd quanta in ν_2 (umbrella mode). Explanation as in Fig. 3.

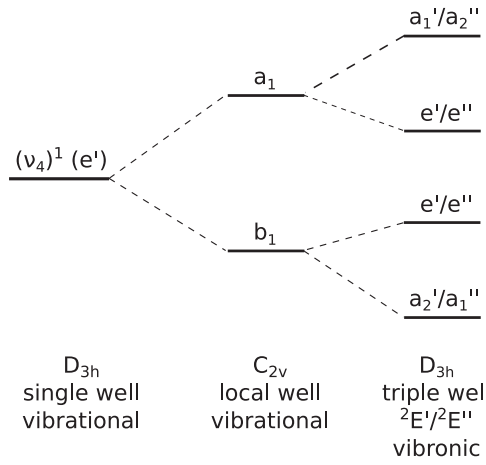

FIG. 5. Schematic level structure corresponding to one quantum in ν_4 (degenerate asymmetric bending mode). Explanation as in Fig. 3.

a vibronic triplet of e' below a_1' because the a_1 local vibration corresponds to a pure radial excitation. The mode-mode combination of ν_1 and ν_4 will lead to an already seen kind of level pattern since ν_1 is totally symmetric in D_{3h} as well as in the local C_{2v} symmetry. Thus, two triplets of vibronic states are obtained with the ordering a_1'' below e'' and e'' below a_2''. Finally, the mode-mode combination of ν_1 and ν_2 will result in the same pattern as a single excitation in ν_2, namely, e' below a_1'. These schemes of level patterns will be very helpful in the analysis of the spectrum simulation in order to analyze the dynamical nature of the vibronic states computed. However, they are deduced from an idealized $E \otimes e$ Jahn-Teller model and the real system may deviate from those patterns.

The level structure of NO_3 as derived by us above is mostly in agreement with the one discussed, for example, in the work of Codd *et al.* in terms of a simple vibronic coupling model.[72] However, comparison with the notation of the levels as indicated by Codd *et al.* must be taken with great caution because the meaning of the *quantum numbers* referring to the tunnelling model is rather different from their use of similar quantum numbers (see above).

We proceed with a systematic analysis of the computed levels ordered by energy. The numerical degeneracy for the lowest triplets is sufficiently good to solve the non-bijective

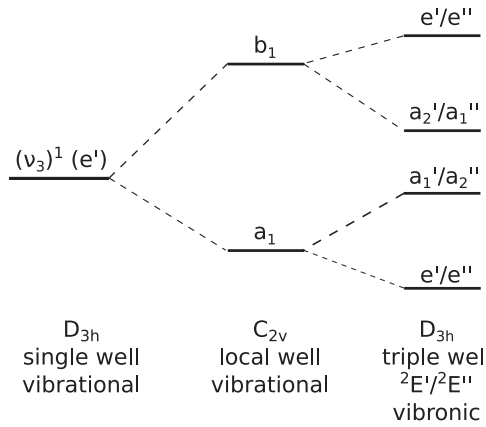

FIG. 6. Schematic level structure corresponding to one quantum in ν_3 (degenerate asymmetric stretching mode). Explanation as in Fig. 3.

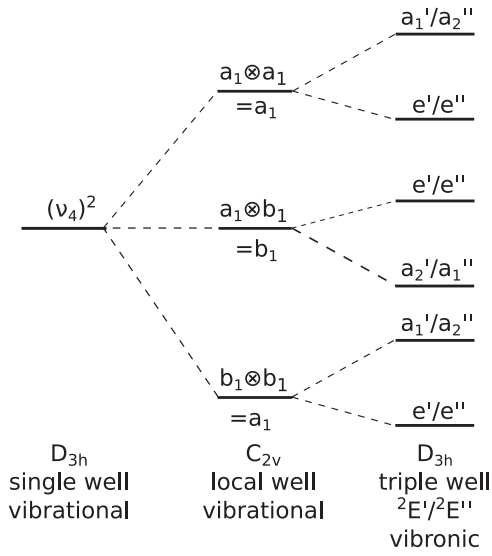

FIG. 7. Schematic level structure corresponding to two quanta in ν_4 (degenerate asymmetric bending mode). Explanation as in Fig. 3.

relation between the $\Gamma_{C_{2v}}$ of the MCTDH calculation and of the correct $\Gamma_{D_{3h}}$ of the system (see Table III). With the various patterns provided in Figures 3–8 as well as the *ab initio* harmonic frequencies' calculation,[57] we could easily assign the few lowest eigenstates. The ground state clearly corresponds to the triplet $1_{\alpha,\beta,\gamma}$. These "keys" $1_{\alpha,\beta,\gamma}$ are given in the first column of Table V. They help to pinpoint the tunnelling triplets of the assignment proposed in the 5th column. The ordering of α, β, γ

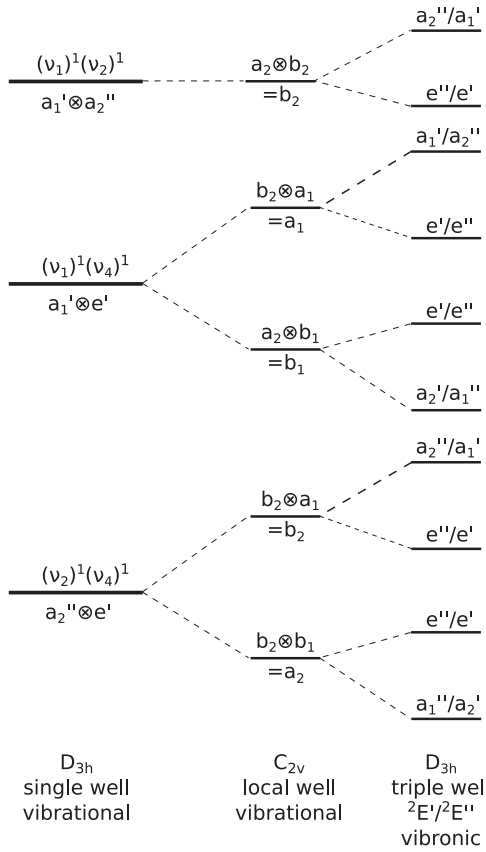

FIG. 8. Schematic level structure corresponding to various combination modes. Explanation as in Fig. 3.

in each triplet is based on energy only and the numbering of the triplets themselves is based on the assignment procedure we followed. The two single excitations in ν_4 are found as triplets $2_{\alpha,\beta,\gamma}$ and $4_{\alpha,\beta,\gamma}$. This assignment minimizes the energy difference between the non-degenerate and the doubly degenerate levels of the same local excitation $4^1(b_1)$ and $4^1(a_1)$. An alternative grouping of the 2 times 3 energies is proposed in the last column of Table V. This alternative assignment follows the level ordering of Fig. 5 for each $4^1(b_1)$ and $4^1(a_1)$ excitation. Triplet $3_{\alpha,\beta,\gamma}$ is assigned to be the excitation in the umbrella out-of-plane mode. The umbrella excitation is clearly anharmonic and the corresponding energies lie in between the two 4^1 triplets. For the next triplet, $5_{\alpha,\beta,\gamma}$, an additional visual inspection of 2D projections of the wave-functions helps to assign this state manifold with confidence to a single excitation in the totally symmetric stretching mode, ν_1. Combination bands including a single excitation of the umbrella mode are identified easily when checking the MCTDH $\Gamma_{C_{2v}}$. The corresponding energies are thus the next ones to label with little ambiguity. The assignments of the triplet $6_{\alpha,\beta,\gamma}$ to $2^1 4^1(a_2)$, the triplet $7_{\alpha,\beta,\gamma}$ to $2^1 4^1(b_2)$, and $8_{\alpha,\beta,\gamma}$ to $1^1 2^1(b_2)$ are thus made based on assuming the minimal tunnelling splittings possible given the symmetry constraints. Due to the noticeable tunnelling splitting of about 20 cm^{-1} and the very high density of states, the two levels of the triplet $6_{\alpha,\beta,\gamma}$ are interlaced by two other states of e'' and a_2'' symmetries, which cannot be assigned with certainty. The triplet $9_{\alpha,\beta,\gamma}$ corresponding at that point to three low energies which are not yet assigned is attributed to the $4^2(a_1)$ double excitation of ν_4 given the e'' below a_1'' pattern. Up to here the assignments are based on a solid analysis of the available data and are made with confidence. All further states cannot be assigned with such certainty because of the very high density of states and the complexity of the 6D wave functions prohibiting a deeper insight into the involved nuclear motions. We nevertheless propose two possibilities of assignments of the remaining energies in the two last columns of Table V, which are based only on vibronic symmetry arguments following the predicted patterns and assumptions about the probable state energies and tunnelling splittings. These tentative assignments are printed in normal face while the sure assignments are indicated by bold face symbols. In the fifth column of the table, we distinguish the two assigned triplets $4^2(a_1)$ (see Fig. 7) by using the ∘ symbol for the upper triplet.

We summarize the tunnelling splittings and the mid-frequencies of the fundamentals in Table VI. The tunnelling splitting of the ground state is remarkably large, amounting to 53 cm^{-1}. The tunnelling splittings of the excited states are strongly dependent on the mode excited. The largest one obtained for one of the unequivocally assigned levels is for the totally symmetric stretch, with a value of 120 cm^{-1}. Excitations in the umbrella mode or in the bending modes reduce the tunnelling splittings by a factor of up to five. Strong differences are observed between the (a_1) and the (b_1) components of 4^1 for the two proposed assignments, which is to be expected given the different orientations of the molecular displacements with respect to the local C_{2v} wells. For the two assignments, $4^1(b_1)$ manifold exhibits a 1.7–2.8 times larger splitting than the $4^1(a_1)$ triplet. For the anti-symmetric stretching mode ν_3, the values resulting from the two propositions of the assignment are given. They correspond to quite different values for both the tunnelling splittings and the mid-frequencies. The values of the tunnelling splittings are quite large, which is reasonable given the effect of stretching modes on the tunnelling splitting as seen for 1^1.

TABLE VI. Tunneling splitting values in cm^{-1} for the ground state and the singly excited vibronic levels and the corresponding mid-frequencies shifted by the ground state mid-frequency value of 17.6 cm^{-1}.

Key	Assignment	ΔE	E_{mid}
$1_{\alpha,\beta,\gamma}$	0	53	0
$5_{\alpha,\beta,\gamma}$	$1^1(a_1)$	120	832
$3_{\alpha,\beta,\gamma}$	$2^1(b_2)$	40	598
	Proposition *i*		
$13_{\alpha,\beta,\gamma}$	$3^1(a_1)$	96	1285
$15_{\alpha,\beta,\gamma}$	$3^1(b_1)$	16	1459
$2_{\alpha,\beta,\gamma}$	$4^1(b_1)$	31	552
$4_{\alpha,\beta,\gamma}$	$4^1(a_1)$	11	632
	Proposition *ii*		
	$3^1(a_1)$	24	1241
	$3^1(b_1)$	108	1354
	$4^1(a_1)$	62	584
	$4^1(b_1)$	105	601

D. Comparison between experiment and theory

According to Fermi's golden rule, the absorption probability (or the transition rate) of a transition is proportional to the absolute square of the transition matrix element $|\langle\Psi_{fn}|\vec{\mu}|\Psi_{im}\rangle|^2$. Often only electric dipole transitions due to $\widehat{\vec{\mu}}_e$ are considered because magnetic dipole transitions due to $\widehat{\vec{\mu}}_m$ or higher moments are generally much weaker. Usually, the states can be represented in terms of electronic (ψ) and nuclear (φ) wave functions yielding for the transition probability

$$p_{fn\leftarrow im} \propto \left(\left|\langle\varphi_n\langle\psi_f|\vec{\mu}_e|\psi_i\rangle\varphi_m\rangle\right|^2 + \left|\langle\varphi_n\langle\psi_f|\vec{\mu}_m|\psi_i\rangle\varphi_m\rangle\right|^2\right) \times \delta(E_f - E_i - h\nu), \quad (6)$$

in which the delta function represents Einstein's resonance condition between initial and final energy levels and the frequency of the light interacting with the molecule. However, as pointed out above, the separation of electronic and vibrational states is inappropriate due to the vibronic coupling in the final states. Therefore, the vibronic states Ψ_{fn} and their symmetries have to be used to analyze the transition probabilities. The symmetry of the system is utilized to identify the vanishing or non-vanishing matrix elements by evaluating the direct products of the irreducible representations Γ of wave functions and operators, which must contain the totally symmetric $\Gamma_{a_1'}$. The operators transform like a_2'' and e' for $\widehat{\vec{\mu}}_e$ and a_2' and e'' for $\widehat{\vec{\mu}}_m$, respectively. The electronic ground state is $^2A_2'$ and we considered the most relevant initial vibrational states which are the ground state of a_1' symmetry or the lowest excited state of e' symmetry. The corresponding

selection rules for the allowed transitions are summarized in Table VII for all possible symmetries of the final vibronic state, the ground vibrational initial state of a_1', and the first excited vibrational initial state of e' symmetry, respectively. This table allows to see easily, which levels can be reached by parallel or perpendicular dipole or magnetic transitions and to match this with the experimental results of Refs. 71 and 72. If we also take into account the next higher electric moment, namely, the quadrupole moment, only one additional symmetry of the final vibronic states would become accessible, which is a_2'. In our calculations, there is only one vibronic state that certainly is of this symmetry, 6_α, which does not match any of the experimental lines better than other states accessible by electric dipole transitions. Quadrupole transitions were not included in the discussion by the experimental groups analysing their CRDS data. We agree with the assessment that quadrupole transitions do not play a role in these experimental spectra.

We first consider the vibronic ground state $1_{\alpha,\beta}$ of e'' symmetry. The 0-0 transition is electric dipole-forbidden but allowed as a perpendicular magnetic dipole transition. On the other hand, the hot band transition 4_1^0 is dipole allowed and parallel. Both types of transitions have been found as very weak and weak signals, respectively, in the CRDS study of Takematsu *et al.*[71] At the temperature of that experiment, the 4^1 vibrational level of the electronic ground state is populated to 20%–30% of the ground state population, explaining why the hot band transition is quite strong compared to the 0-0 line, which is due to the magnetic transition.

We now focus on the dipole allowed transitions into higher vibronic levels. The first of those we find at 549 cm^{-1} above the vibronic ground state (2_α), which we assign to the parallel $4_0^1(b_1)$ transition due to the a_1'' symmetry. The e'' component of this vibronic state triplet could only be reached by a perpendicular magnetic transition from the ground state. Note that this e'' component, however, is accessible as a hot band starting thus from an initially excited NO_3. There are two possibilities to assign the e'' component of the $4_0^1(b_1)$ manifold. The one with the lower tunneling splitting would be at 580 cm^{-1} ($2_{\beta,\gamma}$) but would result in an incompatible level ordering for $4_0^1(a_1)$ (see Fig. 5). By contrast, the compatible assignment at 654 cm^{-1} would lead to considerably larger tunneling splittings (see Table VI). Our result for the dipole allowed transition at 549 cm^{-1} compares very well with the experimental assignment and value of 540 cm^{-1}.[71,72] The next vibronic state, $3_{\alpha,\beta}$, is of e' symmetry and is assigned to the perpendicular dipole transition $2_0^1(b_2)$ at 602 cm^{-1}. The a_1' component, 3_γ, of this vibronic triplet would only be visible as a parallel magnetic transition or as a perpendicular electric hot band transition. The experiments report energies of 678–682 cm^{-1} above 0-0 transition for this state, so the agreement is not that impressive. Note that the diabatic PES model we use for the present calculations does not include the $^2A_2'$ and $^2E'$ electronic states, which couple to the $^2E''$ state through ν_2. Therefore, some deficiencies of the PESs along this mode may be expected. The next five vibronic levels are all dipole-forbidden and thus are not likely to contribute to the experimental spectra. By contrast, the a_1'' state at 1137 cm^{-1} associated with the parallel transition $4_0^2(b_1)$ is dipole-allowed. The computed energy of 1137 cm^{-1} is somewhat higher than the experimental value of 1057 cm^{-1}. What is more peculiar is that the computations obviously predict a negative anharmonicity in contrast to the experimental result. We have no explanation for this discrepancy but the negative anharmonicity of course is easily explained by the broad triple-well structure of the lower adiabatic PES sheet. The four following levels are again dipole-forbidden and are not discussed in detail. The $6_{\beta,\gamma}$ state of e' vibronic symmetry can be reached by a perpendicular dipole transition and is assigned to the combination band $2_0^1 4_0^1(a_2)$ at 1178 cm^{-1} above 0–0. The next dipole-allowed perpendicular transition we find for $2_0^1 4_0^1(b_2)$ corresponding to the e' vibronic state $7_{\alpha,\beta}$ at 1237 cm^{-1}. The corresponding energy obtained from the measured spectrum is 1221 cm^{-1} in reasonable agreement with our calculations for either of those two allowed transitions. It remains an open question why only one of the two levels is observed experimentally. The next transition can be assigned in two ways and our assignments are only tentative. The a_1'' state could be assigned either to the parallel dipole transitions $1_0^1 4_0^1(b_1)$ or $3_0^1(b_1)$, which we find at 1300 cm^{-1}. The experimental value of 1271 cm^{-1} has been assigned to 3_0^1, which would be in agreement with one of the two possibilities. The next dipole allowed state is found at 1408 cm^{-1} and is assigned to the perpendicular transition $1_0^1 2_0^1(b_2)$. An experimentally observed perpendicular transition at 1464 cm^{-1} has been assigned to $1_0^1 2_0^1$ in reasonable agreement with our computation. Finally, one more a_1'' state is computed at 1466 cm^{-1} that corresponds to a parallel dipole transition. We have two tentative assignments for this state, either $3_0^1(b_1)$ or $1_0^1 4_0^1(b_1)$. The experimental spectra do not show any parallel transition between 1297 cm^{-1} and 1603 cm^{-1}, though. The dynamics calculations on our pure *ab initio* PES model yield a quite reasonable agreement with the experimental CRDS observations, confirming most of the assignments made previously. The remaining deviations should be mostly due to the limited accuracy of the *ab initio* calculations on which the diabatic PES model is based. Table VIII summarizes the comparison of the computed and assigned levels with the experimental data.

TABLE VII. Allowed and forbidden electric and magnetic dipole transitions as a function of the final vibronic state symmetries for two initial vibrational states. Allowed transitions are distinguished as parallel (||) or perpendicular (⊥).

$\Gamma_{\Psi_{fn}}$	$\Gamma_{\Psi_{im}}$	$\widehat{\vec{\mu}}_e$	$\widehat{\vec{\mu}}_m$
a_1'	a_2'	0	||
a_2'	a_2'	0	0
e'	a_2'	⊥	0
a_1''	a_2'	||	0
a_2''	a_2'	0	0
e''	a_2'	0	⊥
a_1'	e'	⊥	0
a_2'	e'	⊥	0
e'	e'	⊥	||
a_1''	e'	0	⊥
a_2''	e'	0	⊥
e''	e'	||	⊥

TABLE VIII. Summary of the comparison between experimental and computed transitions. The first 4 columns report the data of Table VI of Ref. 72 together with our theoretical energies obtained for these assignments. Energies in cm^{-1} are followed by the deviation to the experimental values. In columns "Case 1" and "Case 2," we propose two alternative assignments based on the computed energies and eigenstate analysis. The parallel (∥) or perpendicular (⊥) character of the unobserved levels are also given.

Assignment of Ref. 72				Case 1		Case 2	
E_{exp}	Type	Label experiment	E_{th}	Energy	Assignment	Energy	Assignment
540	∥	4_0^1	549 (9)	549 (9)	$4_0^1(b_1)$	549 (9)	$4_0^1(b_1)$
682	⊥	2_0^1	602 (80)	602 (80)	$2_0^1(b_2)$	602 (80)	$2_0^1(b_2)$
1057	∥	4_0^2	1137 (80)	1137 (80)	$4_0^2(b_1)$	1137 (80)	$4_0^2(b_1)$
				1178 (⊥)	$2_0^1 4_0^1(a_2)$	1178 (⊥)	$2_0^1 4_0^1(a_2)$
1221	⊥	$2_0^1 4_0^1$	1178 (43)	1237 (16)	$2_0^1 4_0^1(b_2)$	1237 (16)	$2_0^1 4_0^1(b_2)$
1271	∥	3_0^1	1300 (29)	1300 (29)	$1_0^1 4_0^1(b_1)$	1300 (29)	$3_0^1(b_1)$
1464	⊥	$1_0^1 2_0^1$	1407 (57)	1407 (57)	$1_0^1 2_0^1(b_2)$	1407 (57)	$1_0^1 2_0^1(b_2)$
				1466 (∥)	$3_0^1(b_1)$	1466 (∥)	$1_0^1 4_0^1(b_1)$

IV. CONCLUSION

In the present study, the vibronic eigenstates of the first electronically excited $^2E''$ state of the NO_3 radical and the vibrational eigenstates of the NO_3^- anion electronic ground state have been investigated thoroughly. Special attention has been paid to an understanding of the states in terms of symmetry and of the topography of the PESs, respectively, as well as the influence of tunnelling and the geometric phase effect. To this end, first the lowest 41 vibrational levels of NO_3^- have been computed with two different approaches, namely, a time-independent DVR computation using a harmonic oscillator basis expansion and the MCTDH based state average and block diagonalization approach. All states have been analyzed and assigned in terms of excitations and state symmetry. For the higher excitations, an analysis of the symmetrized harmonic oscillator basis is particularly helpful for these assignments. The results are compared to those of an earlier study of the vibrational levels of the electronic ground state of neutral NO_3. The same types of low-lying vibrational states are observed because both systems are represented by a single-sheeted PES with a single D_{3h} symmetric potential minimum. However, we note that much lower frequencies for the radical and a different anharmonicity is found for the two asymmetric e' modes, ν_3 and ν_4, when compared to the anion. We also observe that the splittings between the different states arising from higher excitations of e' modes, e.g., a_1', a_2', and e' corresponding to a 3^3 or 4^3 configuration, are very different between the anion and neutral system. It appears that the radical is much more easily deformed asymmetrically along the ν_3 and ν_4 modes than the anion, which can be explained by a strong *pseudo*-Jahn-Teller coupling to the second excited state of $^2E'$ symmetry, an interaction which is certainly not present in the anion. Since the 3^1 fundamental found for the anion is 1353 cm^{-1} according to our calculations, it is very reasonable to assume that the corresponding fundamental for the radical will be even lower, in agreement with previous calculations of Stanton. This strengthens the interpretation that the band at 1492 cm^{-1} observed experimentally for the radical cannot be due to this fundamental but must be a combination band.

In a second step, vibronic levels of the NO_3 radical in the $^2E''$ electronic state have been determined accurately. The computation is carried out using a diabatic representation of the electronic two-sheeted $^2E''$ state potential previously derived by us and the MCTDH algorithm is utilized to solve the corresponding vibronic Schrödinger equation in full dimensionality. Due to the strong vibronic coupling present in this state, the level structure is very different compared to that of the anion or the $^2A_2'$ ground state of the radical. An interpretation of the computed levels is proposed based on a simple model. It relies on a local separation of the electronic and vibrational degrees of freedom, on a model of the tunnelling effect due to the topography of the lower adiabatic PES sheet, and on the symmetrization of localized wave functions to yield the correct vibronic eigenstates. The vibronic coupling leads to three equivalent potential wells on the lower adiabatic PES sheet, which are connected by rather low barriers to *pseudo*-rotation. Each of the wells only shows a local symmetry of C_{2v}, though the global symmetry of the PES is D_{3h} of course. This leads to a splitting of vibrational modes corresponding to e' vibrations in the conventional D_{3h} sense. The symmetrization over the local wells results in tunnelling triplets of vibronic states of symmetries a_1' or a_2' and e' or alternatively a_1'' or a_2'' and e'' each. Whenever formally e' symmetric modes like ν_3 or ν_4 are involved, the geometric phase effect has to be accounted for, which alters the succession of a and e states depending on the excitation.

With this scheme, we can firmly assign 8 triplets (thus 24 energies, 8 of them doubly degenerate). They correspond to the ground state but also to excitations of the umbrella, the totally symmetric and/or the bending asymmetric modes. Quite large and mode specific tunnelling splittings are obtained. From symmetry considerations of the transition probabilities, we found that these tunnelling splittings are not directly observable experimentally with electric dipole transitions from the ground state of $^2A_2'$. Some of them are, however, accessible when considering hot band transitions with an initial state excitation in an e' mode. Experimental access to magnetic transitions also would be of great value to verify our predictions on the tunnelling splittings.

The numerical results and theoretical assignments are compared to experimental results from a jet-cooled cavity ring-down spectroscopy study. We assign the transitions $4_0^1(b_1)$, $2_0^1(b_2)$, $4_0^2(b_1)$, $2_1^1 4_0^1(b_2)$, and $1_0^1 2_0^1(b_2)$ in agreement with the experiment and with deviations between 9 and 80 cm^{-1} in the level energies. One level assigned experimentally to 3_0^1 could be assigned from our theoretical results either to $1_0^1 4_0^1(b_1)$ or to $3_0^1(b_1)$. Given the tremendous difficulties in both electronic structure calculations and PES development, this seems to be a quite satisfactory result.

For a more accurate comparison with the CRDS spectra, a representation of the electronic ground $^2A_2'$ surface is mandatory. However, this electronic state is coupled to the $^2E'$ second excited state and both of them are coupled to the $^2E''$ state, thus a five-sheeted potential surface is required. Work on getting such a representation of NO_3 is currently in progress in our groups.

SUPPLEMENTARY MATERIAL

See supplementary material for graphical representations of key features of the NO_3 PESs, evidence for the proposed tunnelling model, and detailed derivations of the level ordering.

ACKNOWLEDGMENTS

The authors acknowledge the generous financial support via the UFA-DFH organization. This work has been also supported by the University of Rennes 1 via the grant "Action Incitative: Activité internationale 2014" and via the INTEGER project included in the No. EU 7ePC/2007-2013 program with the Convention No. 266638. We thank Uwe Manthe, Terry Miller, and Mitchio Okumura for many fruitful and conducive discussions.

[1] *Conical Intersections: Electronic Structure, Dynamics and Spectroscopy*, edited by W. Domcke, D. R. Yarkony, and H. Köppel (World Scientific, Singapore, 2004).
[2] H. C. Longuet-Higgins, Adv. Spectrosc. **2**, 429 (1961).
[3] W. Lichten, Phys. Rev. **131**, 229 (1963).
[4] W. Lichten, Phys. Rev. **164**, 131 (1967).
[5] F. T. Smith, Phys. Rev. **179**, 111 (1969).
[6] M. Baer, Chem. Phys. **15**, 49 (1976).
[7] C. A. Mead and D. G. Truhlar, J. Chem. Phys. **77**, 6090 (1982).
[8] C. A. Mead, J. Chem. Phys. **78**, 807 (1983).
[9] T. Pacher, L. S. Cederbaum, and H. Köppel, J. Chem. Phys. **89**, 7367 (1988).
[10] T. Pacher, C. A. Mead, L. S. Cederbaum, and H. Köppel, J. Chem. Phys. **91**, 7057 (1989).
[11] T. Pacher, H. Köppel, and L. S. Cederbaum, J. Chem. Phys. **95**, 6668 (1991).
[12] T. Pacher, L. S. Cederbaum, and H. Köppel, Adv. Chem. Phys. **84**, 293 (1993).
[13] H. Köppel, W. Domcke, and L. S. Cederbaum, Adv. Chem. Phys. **57**, 59 (1984).
[14] R. Cimiraglia, J. P. Malrieu, M. Persico, and F. Spiegelmann, J. Phys. B: At. Mol. Phys. **18**, 3073 (1985).
[15] W. Domcke and C. Woywod, Chem. Phys. Lett. **216**, 362 (1993).
[16] G. J. Atchity and K. Ruedenberg, Theor. Chem. Acc. **97**, 47 (1997).
[17] H. Nakamura and D. G. Truhlar, J. Chem. Phys. **115**, 10353 (2001).
[18] H. Nakamura and D. G. Truhlar, J. Chem. Phys. **117**, 5576 (2002).
[19] H. Nakamura and D. G. Truhlar, J. Chem. Phys. **118**, 6816 (2003).
[20] M. S. Schuurman and D. R. Yarkony, J. Chem. Phys. **127**, 094104 (2007).
[21] B. N. Papas, M. S. Schuurman, and D. R. Yarkony, J. Chem. Phys. **129**, 124104 (2008).
[22] X. Zhu and D. R. Yarkony, J. Chem. Phys. **130**, 234108 (2009).
[23] X. Zhu and D. R. Yarkony, J. Chem. Phys. **132**, 104101 (2010).
[24] X. Zhu and D. R. Yarkony, J. Chem. Phys. **136**, 174110 (2012).
[25] H. Ndome, R. Welsch, and W. Eisfeld, J. Chem. Phys. **136**, 034103 (2012).
[26] H. Ndome and W. Eisfeld, J. Chem. Phys. **137**, 064101 (2012).
[27] N. Wittenbrink, H. Ndome, and W. Eisfeld, J. Phys. Chem. A **117**, 7408 (2013).
[28] F. Venghaus and W. Eisfeld, J. Chem. Phys. **144**, 114110 (2016).
[29] A. J. C. Varandas, F. B. Brown, C. A. Mead, D. G. Truhlar, and N. C. Blais, J. Chem. Phys. **86**, 6258 (1987).
[30] H.-J. Werner, B. Follmeg, and M. H. Alexander, J. Chem. Phys. **89**, 3139 (1988).
[31] H. Werner and W. Meyer, J. Chem. Phys. **74**, 5802 (1981).
[32] G. Hirsch, R. J. Buenker, and C. Petrongolo, Mol. Phys. **70**, 835 (1990).
[33] B. Heumann, K. Weide, R. Düren, and R. Schinke, J. Chem. Phys. **98**, 5508 (1993).
[34] D. Simah, B. Hartke, and H. Werner, J. Chem. Phys. **111**, 4523 (1999).
[35] A. Dobbyn, J. Connor, N. Besley, P. Knowles, and G. Schatz, Phys. Chem. Chem. Phys. **1**, 957 (1999).
[36] M. Hoffmann and G. Schatz, J. Chem. Phys. **113**, 9456 (2000).
[37] P. Cattaneo and M. Persico, Theor. Chem. Acc. **103**, 390 (2000).
[38] R. P. Krawczyk, A. Viel, U. Manthe, and W. Domcke, J. Chem. Phys. **119**, 1397 (2003).
[39] C. R. Evenhuis and M. A. Collins, J. Chem. Phys. **121**, 2515 (2004).
[40] C. R. Evenhuis, X. Lin, D. H. Zhang, D. Yarkony, and M. A. Collins, J. Chem. Phys. **123**, 134110 (2005).
[41] O. Godsi, C. R. Evenhuis, and M. A. Collins, J. Chem. Phys. **125**, 104105 (2006).
[42] A. Viel and W. Eisfeld, J. Chem. Phys. **120**, 4603 (2004).
[43] W. Eisfeld and A. Viel, J. Chem. Phys. **122**, 204317 (2005).
[44] A. V. Marenich and J. E. Boggs, J. Chem. Phys. **122**, 024308 (2005).
[45] A. V. Marenich and J. E. Boggs, Chem. Phys. Lett. **404**, 351 (2005).
[46] A. Viel, W. Eisfeld, S. Neumann, W. Domcke, and U. Manthe, J. Chem. Phys. **124**, 214306 (2006).
[47] A. Viel, W. Eisfeld, C. R. Evenhuis, and U. Manthe, Chem. Phys. **347**, 331 (2008).
[48] V. C. Mota and A. J. C. Varandas, J. Phys. Chem. A **112**, 3768 (2008).
[49] D. Opalka and W. Domcke, Chem. Phys. Lett. **494**, 134 (2010).
[50] D. Opalka and W. Domcke, J. Chem. Phys. **132**, 154108 (2010).
[51] X. Zhu, J. Y. Ma, D. R. Yarkony, and H. Guo, J. Chem. Phys. **136**, 234301 (2012).
[52] J. Ma, X. Zhu, H. Guo, and D. R. Yarkony, J. Chem. Phys. **137**, 22A541 (2012).
[53] X. Zhu and D. R. Yarkony, J. Chem. Phys. **140**, 024112 (2014).
[54] N. Wittenbrink, F. Venghaus, D. Williams, and W. Eisfeld, J. Chem. Phys. **145**, 184108 (2016).
[55] W. Eisfeld, O. Vieuxmaire, and A. Viel, J. Chem. Phys. **140**, 224109 (2014).
[56] R. P. Wayne, I. Barnes, P. Biggs, J. P. Burrows, C. E. Canosamas, J. Hjorth, G. Lebras, G. K. Moortgat, D. Perner, G. Poulet *et al.*, Atmos. Environ., Part A **25**, 1 (1991).
[57] W. Eisfeld and K. Morokuma, J. Chem. Phys. **113**, 5587 (2000).
[58] W. Eisfeld and K. Morokuma, J. Chem. Phys. **114**, 9430 (2001).
[59] W. Eisfeld and K. Morokuma, J. Chem. Phys. **119**, 4682 (2003).
[60] M. Mayer, L. S. Cederbaum, and H. Köppel, J. Chem. Phys. **100**, 899 (1994).
[61] J. F. Stanton, J. Chem. Phys. **126**, 134309 (2007).
[62] C. S. Simmons, T. Ichino, and J. F. Stanton, J. Phys. Chem. Lett. **3**, 1946 (2012).
[63] S. Mahapatra, W. Eisfeld, and H. Köppel, Chem. Phys. Lett. **441**, 7 (2007).
[64] S. Faraji, H. Köppel, W. Eisfeld, and S. Mahapatra, Chem. Phys. **347**, 110 (2008).
[65] J. F. Stanton, Mol. Phys. **107**, 1059 (2009).
[66] J. F. Stanton and M. Okumura, Phys. Chem. Chem. Phys. **11**, 4742 (2009).
[67] A. D. Walsh, J. Chem. Soc. **1953**, 2301.
[68] A. Weaver, D. W. Arnold, S. E. Bradforth, and D. M. Neumark, J. Chem. Phys. **94**, 1740 (1991).
[69] A. Deev, J. Sommar, and M. Okumura, J. Chem. Phys. **122**, 224305 (2005).
[70] M. Okumura, J. Stanton, A. Deev, and J. Sommar, Phys. Scr. **73**, C64 (2006).
[71] K. Takematsu, N. C. Eddingsaas, D. J. Robichaud, and M. Okumura, Chem. Phys. Lett. **555**, 57 (2013).
[72] T. Codd, M.-W. Chen, M. Roudjane, J. F. Stanton, and T. A. Miller, J. Chem. Phys. **142**, 184305 (2015).
[73] M. E. Jacox and W. E. Thompson, J. Phys. Chem. A **114**, 4712 (2010).
[74] D. Xiao, M.-C. Chang, and Q. Niu, Rev. Mod. Phys. **82**, 1959 (2010).

[75]H. D. Meyer, U. Manthe, and L. S. Cederbaum, Chem. Phys. Lett. **165**, 73 (1990).
[76]U. Manthe, H. D. Meyer, and L. S. Cederbaum, J. Chem. Phys. **97**, 3199 (1992).
[77]U. Manthe, J. Chem. Phys. **128**, 064108 (2008).
[78]G. Schiffel and U. Manthe, J. Chem. Phys. **132**, 084103 (2010).
[79]R. Wodraszka, J. Palma, and U. Manthe, J. Phys. Chem. A **116**, 11249 (2012).
[80]C. Evenhuis, G. Nyman, and U. Manthe, J. Chem. Phys. **127**, 144302 (2007).
[81]U. Manthe, J. Chem. Phys. **105**, 6989 (1996).
[82]J. C. Light and T. Carrington, Adv. Chem. Phys. **114**, 263 (2000).
[83]C. Leonard, S. Carter, and N. C. Handy, Chem. Phys. Lett. **370**, 360 (2003).
[84]R. Marquardt, K. Sagui, J. J. Zheng, W. Thiel, D. Luckhaus, S. Yurchenko, F. Mariotti, and M. Quack, J. Phys. Chem. A **117**, 7502 (2013).
[85]F. S. Ham, Phys. Rev. Lett. **58**, 725 (1987).
[86]W. Englman, *The Jahn-Teller Effect in Molecules and Crystals* (Wiley-Interscience, London, 1972).